Nucleic Acids Research, 2026, **54**, gkaf1487
https://doi.org/10.1093/nar/gkaf1487
Genome integrity, repair and replication

Transcription termination counteracts DNA damage after WEE1 inhibition

Helga B Landsverk[1], Lise E Sandquist[1], Lilli TE Bay[1], Sissel Hauge[1], Linda van Bijsterveldt[2,3], Lilian Lindbergsengen[1], Christin Lund-Andersen[4], Chakravarthi Kanduri[5], Heidi Lyng[1,6], Christina S Fjeldbo[1], Tord Hompland[1], Timothy C Humphrey[2,7], Randi G Syljuåsen[1,*]

[1]Department of Radiation Biology, Institute for Cancer Research, Oslo University Hospital, 0379 Oslo, Norway
[2]Department of Oncology, Medical Sciences Division, University of Oxford, Oxford OX3 7DQ, UK
[3]MRC Laboratory of Molecular Biology, Cambridge CB2 0QH, UK
[4]Department of Tumor Biology, Institute for Cancer Research, Oslo University Hospital, 0379 Oslo, Norway
[5]Department of Informatics, University of Oslo, 0373 Oslo, Norway
[6]Department of Physics, University of Oslo, 0371 Oslo, Norway
[7]Genome Damage and Stability Centre, University of Sussex, Brighton, East Sussex BN1 9RQ, UK

*To whom correspondence should be addressed. Email: ransyl@ous-hf.no

Abstract

Transcription termination is a key regulatory step in transcription and a potential target for cancer therapy, but how it can be exploited for treatment is incompletely understood. Here we show that transcription termination plays a crucial role in mitigating DNA damage and cell death upon WEE1 inhibition by adavosertib. Depleting five different transcription termination factors (WDR82, PNUTS, XRN2, DDX5, or CPSF73) increased adavosertib-induced DNA damage in S-phase. Conversely, inhibiting active transcription with DRB or triptolide, or co-depleting CDC73, a component of the PAF1 transcription elongation complex, reduced such damage. Additionally, read-through transcription following WDR82 depletion was partially inhibited by co-depletion of CDC73, supporting that read-through transcription contributes to DNA damage in response to WEE1 inhibition. Moreover, combining adavosertib with the CPSF73 inhibitor JTE-607, an anticancer compound which promotes read-through transcription, increased DNA damage during S-phase. Elevated expression of CPSF73 is associated with aggressive disease in prostate cancer patients, and combining JTE-607 with adavosertib synergistically reduced prostate cancer cell survival. Our findings suggest that transcription termination helps prevent toxic conflicts between transcription and replication following increased replication initiation caused by WEE1 inhibition.

Graphical abstract

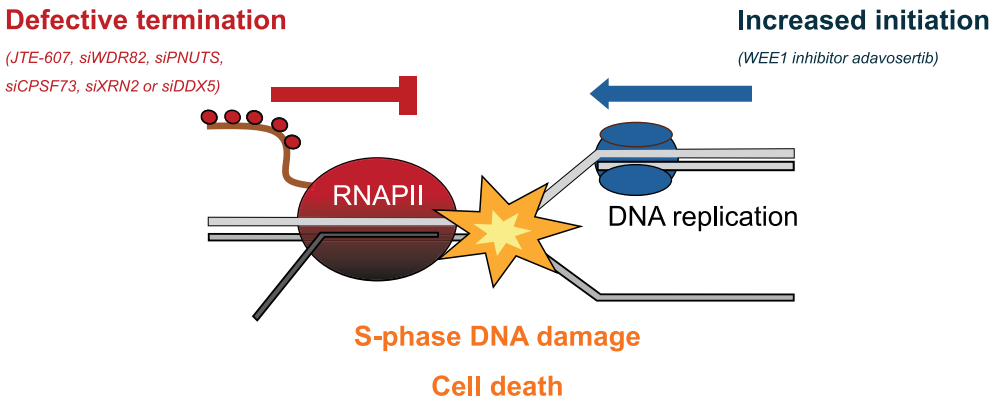

Introduction

As transcription and replication take place on the same template, conflicts can occur. Such transcription-replication conflicts (T-R conflicts) can lead to replication stress and DNA damage and are thus a source of genome instability [1]. Cancer cells frequently display higher levels of T-R conflicts than normal cells [2]. Moreover, some studies suggest T-R conflicts can be exploited for cancer therapy [3, 4]. Nevertheless, the

Received: September 6, 2024. **Revised:** December 4, 2025. **Accepted:** December 11, 2025

mechanisms regulating T-R conflicts are not fully understood, and knowledge regarding how T-R conflicts can be targeted in cancer remains limited.

Several cancer drugs act by inducing excessive replication stress, resulting in DNA damage and cell death [5]. An example is the WEE1 inhibitor adavosertib (also known as MK1775 and AZD1775), which is thought to induce replication stress by enhancing CDK1/2 activity, leading to increased replication initiation and subsequent DNA damage [6, 7]. Whether WEE1 inhibition also enhances T-R conflicts has not yet been addressed, but is likely as increased origin firing has been associated with T-R conflicts after overexpression of Cyclin E [8]. Since adavosertib has been evaluated in clinical trials for various types of cancer, including prostate cancer (e.g. [9]), and two additional WEE1 inhibitors have recently entered clinical trials (e.g. NCT06364410 and NCT06260514), understanding how WEE1 inhibition induces DNA damage and promotes cancer cell death is of great significance.

The occurrence of T-R conflicts is restricted by a variety of mechanisms, including careful regulation of the transcription cycle itself. Interestingly, the process of transcription termination may play a critical role, as inhibition of the *Escherichia coli* transcription termination factor Rho led to replication-dependent DNA damage [10]. Notably, transcription termination is not only prevalent at the end of genes, but occurs throughout the transcription cycle, and in addition ceases pervasive transcription outside protein-coding genes [11–13]. Termination is thus an important mechanism to restrict transcription throughout transcribed areas of the genome, and can occur via several mechanisms in human cells. In protein-coding genes, the cleavage and polyadenylation complex plays a central role in termination by recognizing and cleaving the polyadenylation sequence at the end of the transcribed region [11]. As cryptic polyadenylation sites are present at gene-internal regions, this complex also regulates premature termination [12]. The cleavage and polyadenylation complex component CPSF73 is the key endonuclease involved [14]. Another important enzyme is the exonuclease XRN2, which acts as a torpedo by digesting the nascent RNA after cleavage, leading to transcription termination [11]. RNA:DNA helicases such as Senataxin and DDX5 have also been shown to contribute to termination [15, 16]. In addition, the speed of RNA polymerase II (RNAPII) elongation can regulate termination, as termination factors such as protein phosphatase 1 (PP1) nuclear targeting subunit (PNUTS)-PP1 promote termination by slowing down elongation [17]. The PNUTS binding partner WDR82 [18] also plays a role in termination [19, 20]. RNAPII elongation and termination are believed to be in kinetic competition, as slower elongation leads to shorter, and faster elongation leads to longer, transcribed units [21].

We hypothesized that dynamic regulation of transcription termination may be crucial to avoid T-R conflicts upon increased replication initiation following WEE1 inhibition. Here we provide evidence that adavosertib-induced DNA damage in S-phase is enhanced when transcription termination is suppressed by siRNA-mediated downregulation of termination factors (PNUTS, WDR82, XRN2, DDX5, and CPSF73) or the CPSF73-inhibitor JTE-607. Furthermore, depletion of the transcription elongation factor CDC73 or inhibitors of active transcription partially rescues such damage. As combinations of JTE-607 and adavosertib synergistically reduce cell survival, our results suggest we have discovered a new way to target T-R conflicts for cancer treatment. Moreover, as we find that higher levels of the JTE-607 target CPSF73 are associated with aggressive disease in prostate cancer, this treatment strategy may hold particular relevance for this malignancy.

Materials and methods

Cell lines

Human cervical cancer HeLa Kyoto and osteosarcoma U2OS cells were grown in Dulbecco's modified Eagle's medium (DMEM) and human prostate cancer DU145 and PC3 cells in Roswell Park Memorial Institute (RPMI) 1640 medium, supplemented with antibiotics and 10% fetal bovine serum, at 37°C, 20% O_2, and 5% CO_2 in a humidified incubator. Throughout the manuscript, HeLa Kyoto (HeLa) cells were used unless otherwise stated. The cell lines were authenticated by short tandem repeat profiling using Powerplex 16 (Promega) and were routinely tested for mycoplasma contamination. The WDR82-res HeLa cells stably expressing untagged siRNA-resistant WDR82 were previously described [22].

Chemicals and treatments

The WEE1 inhibitor adavosertib (AZD1775, Selleck Biochem) and the CPSF73 inhibitor JTE-607 (MedChemExpress) were used at indicated concentrations, the CDK9 inhibitor 5,6-dichloro-1-beta-ribo-furanosyl benzimidazole (DRB) (Sigma Aldrich) was used at 100 μM, the CDK7-inhibitor THZ1 (ApexBio) at 1 μM, the XPB inhibitor Triptolide (TPL) (Sigma Aldrich) at 1 μM, and the CHK1 inhibitor AZD7762 (Selleckchem) at 300 nM. Unless otherwise specified in the figure legend, inhibitors were present until harvest.

siRNA transfections

Sequences of siRNA oligonucleotides can be found in the Supplementary Table 1. siRNA was transfected using RNAimax (Life Technologies). Experiments were performed 48–72 h after siRNA transfection.

Western blotting and antibodies

Quantitative western blotting was performed as previously described [22]. Briefly, cells were resuspended in ice-cold TX-100 buffer (100 mM NaCl, 50 mM Tris pH 7.5, 2 mM MgCl2, 0.5% TX-100) containing 100 U/ml Benzonase (Sigma-Aldrich), Complete EDTA-free Protease Inhibitor Cocktail (Merck), and PhosSTOP phosphatase inhibitors (Merck). After 24 h incubation at 4°C, Lane Marker Reducing Sample Buffer (Pierce Biotechnologies) was added, and samples were boiled (95°C, 5 min). Criterion Stain-Free TGX gels (BioRad) and nitrocellulose membranes (BioRad) were used for separation and transfer. Antibodies used can be found in Supplementary Table 2. Blots were imaged in a Chemidoc MP (BioRad) using chemiluminescence substrates (Supersignal west pico, dura or femto; Thermo Scientific). Quantifications were performed and images processed in Image Lab 4.1 (BioRad) software. The range of detection was verified by including a dilution series of one sample, and any saturated signals were excluded. The resulting standard curve allowed accurate quantification. To blot the same membranes several

times with different antibodies, membranes were stripped using ReBlot Plus Mild Antibody Stripping Solution (Millipore).

Flow cytometry analysis

For flow cytometry of whole cells, cells were fixed in ice-cold (-20°C) 70% ethanol. For extracted cells, extraction and fixation were performed as previously described [23]. Briefly, cells were harvested, pelleted and soluble factors were released with 100 µl extraction buffer (20 mM HEPES (pH 7.9), 1.5 mM MgCl2, 140 mM NaCl, 300 mM Sucrose, 0.5% TX-100, Complete EDTA-free Protease Inhibitor Cocktail (Merck), PhosSTOP phosphatase inhibitors (Merck) and 20 µM MG132 (Sigma Aldrich)) for 5 min on ice. Extracted cells were then fixed by the addition of 900 µl formalin solution (Sigma Aldrich). In most experiments, barcoded cells, which provide an internal standard for normalization of the signals from the antibodies, were included during staining. Barcoding was performed as previously described [23]. Briefly, untreated cells (either extracted or whole cells, depending on the experiment) were resuspended in 0,25 µg/ml Alexa Fluor 647 NHS Ester (Thermo Fisher, catalog number: A20006) in PBS and left for 30 min. The barcoding reaction was quenched by adding 5 mL of PBS with 5% fetal bovine serum (FBS). The barcoded cells were next spun down (2000 rpm, 5 min), resuspended in PBS with 5% FBS, and distributed evenly into all the samples. Staining with primary and secondary antibodies was performed as previously described [23]. Briefly, cells were permeabilized with flow buffer (0.1% Igepal CA-630, 6.5 mM Na2HPO4, 1.5 mM KH2PO4, 2.7 mM KCl, 137 mM NaCl, 0.5 mM ethylenediaminetetraacetic acid (pH 7.5)) containing 4% non-fat milk, and stained with primary and secondary antibodies in flow buffer. Antibodies used can be found in Supplementary Table 2. Analysis was performed on an LSRII flow cytometer (BD Biosciences) using Diva and FlowJo software.

Chromatin RNA sequencing

For chromatin RNA sequencing, cells were harvested and washed in PBS. Soluble RNA was released by resuspending the cell pellet in ice-cold extraction buffer (described above) with 1U/µl of RNAse inhibitor (New England Biolabs) and incubating on ice for 5 min. Extracted cells were spun down at 1300 g for 4 min and lysed in Qiazol (Qiagen). Cells were shredded using the QIAshredder homogenizer and separated into organic and aqueous phases after the addition of chloroform and spinning in phase lock gel tubes (Tiangen). Ethanol was added to the aqueous phase containing RNA, and the RNA was collected in RNeasy Mini kit columns (Qiagen). RNA was washed and diluted according to the RNeasy kit protocol. The quality of RNA was verified using a nanodrop and by bioanalyser measurements. Illumina Stranded Total RNA Prep Ligation with Ribo-Zero Plus was used for library preparation. Samples were paired-end sequenced using Illumina NovaSeq6000. Raw data have been deposited in the GEO database (accession number: GSE312256).

Readthrough characterization and analysis

Read mapping of the paired-end RNAseq libraries was carried out using the STAR alignment tool [24]. GRCh38.p13 reference genome version was used for the mapping together with Gencode v38 full annotation. Quantification of readthrough levels was carried out using ARTDeco [25]. Genes with the biggest difference in readthrough between WDR82-depleted cells and scrambled control were inspected and visualized with Integrative Genomics Viewer (IGV) using the GRCh38/hg38 genome reference. Readthrough levels of either the top 2000 expressed genes or all expressed genes were compared across individual libraries. Expressed genes were defined as those with FPKM > 1, a commonly accepted threshold in the field. From the expressed genes, we further selected genes with detectable read density in the read-through region (Log2Ratio > −5). In a more stringent subset, we selected genes with substantial read-through transcription, where the read-through level was comparable to or exceeded that in the gene body region (Log2Ratio > −2). For each of these genes, we computed the proportion of reads containing the canonical polyA signal (AAUAAA), corresponding to AATAAA on the forward strand and TTTATT on the reverse strand in cDNA sequences, separately for gene body and read-through regions. Read-through regions were defined as the 10 kb immediately downstream of the annotated gene body, truncated if another annotated gene occurred within 10 kb, and excluding any overlapping regions. Reads were assigned to either the gene body or read-through region only if at least 90% of their length overlapped the target region.

Proximity ligation assay (PLA) and immunofluorescence microscopy

For PLA assays, cells seeded on glass coverslips were treated with JTE-607 (1 µM, 4 h) and/or adavosertib (1 µM, added during the last 20 min before harvest). For immunofluorescence analysis in Supplementary Fig. S1B, cells were treated with adavosertib 48 h after siRNA transfection. Cells were pre-extracted with detergent buffer (1M Hepes pH 7.9, 0.1 M $MgCl_2$, 50 mM NaCl, 2.5 M sucrose, 0.5% Triton X-100) for 5 min on ice to remove soluble proteins, and fixed with 100% ice-cold methanol for 10 min. The PLA assay was done according to the manufacturer's protocol using rabbit anti-pRNAPII S2 (A311-654A, ThermoFisher Scientific (Bethyl); 1:2000) or rabbit-pRNAPII S5 (ab5131, Abcam; at 1:10 000), in combination with mouse anti-PCNA (PC10, sc-56, Santa Cruz Biotechnology, Inc.; 1:1000). Duolink® In Situ PLA® Probe Anti-Rabbit MINUS (DUO92005; Merck/Sigma) and Anti-Mouse PLUS (DUO92001; Merck/Sigma), together with Detection Reagents Green (DUO92014; Merck/Sigma) were used, and the polymerase amplification time was 120 min. Following the amplification step, cells were incubated with Alexa Fluor 568 Donkey Anti-Mouse IgG (A10037; ThermoFisher; 1:1000) for 30 min at room temperature to detect S-phase cells (containing chromatin-bound PCNA). Immunofluorescence analysis in Supplementary Fig. S1B was performed using antibodies against γH2AX and PCNA, followed by staining with Alexa Fluor 568 donkey anti–mouse IgG and Alexa Fluor 488 donkey anti–rabbit IgG (A21206; ThermoFisher). Cells were stained with the DNA stain Hoechst 33 258 (B1155; Sigma-Aldrich) and mounted with ProLong Diamond Antifade Mountant (P36965; ThermoFisher). Images were acquired using a spinning-disk confocal microscope (Nikon ECLIPSE Ti2-E inverted microscope equipped with a CrestOptics X-Light V3 spinning-disk confocal module) with a 60 × oil-immersion objective. PLA foci were counted in Hoechst-positive nuclei using NIS-Elements AR software (Nikon). S-phase cells were identified based on PCNA levels.

For each treatment, at least 150 S-phase cells were analyzed per experiment.

Viability assay (CellTiterGlo)

Cells were seeded in 96-well microplates (Nunc™, VWR) at a density of 500 (HeLa), 750 (DU145), or 1000 (PC-3) cells/well. The next day, cells were treated with inhibitors using a Tecan D300e digital dispenser (Bergman Diagnostika). When indicated in the figure legend, inhibitors were removed 24 h later, cells were washed once with PBS, and fresh medium without inhibitors was added. Otherwise, the inhibitors were present in the growth medium until the end of the experiment. Five to six days after treatment, the CellTiter-Glo assay (Promega, Madison, WI, USA) was used to measure metabolic activity as a readout for viable cells, according to the manufacturer's protocol. Luminescence was read in a Tecan Spark multimode microplate reader with integration time set to 1 s. In each experiment, the average luminescence values from duplicate wells were obtained, and the viable fraction was calculated by dividing by the average luminescence value of the non-treated samples. Synergy was determined via Bliss independence using the fraction affected of treated cells (Fa = 1-viable fraction). The expected effect of the combination (for additive effects) is:

($Fa_{adavosertib} + Fa_{JTE\text{-}607}$ - ($Fa_{adavosertib}$ x $Fa_{JTE\text{-}607}$)). Excess over Bliss, calculated as the difference between the measured and expected effect, was termed "synergy score" and plotted on surface charts using matplotlib in Python. Statistical significance ($P < 0.05$) was determined via a one-sample one-tailed Student t test. Test criterion: Synergy score > 0.

Clonogenic survival assay

HeLa, PC3, and DU145 cells were seeded at low density (250–500 cells per 6-cm dish; triplicates) and treated 16–20 h later with adavosertib and/or JTE-607. For HeLa cells, cultures were washed with PBS 24 h after treatment, and fresh medium was added. After 12–14 days, colonies were fixed with 70% ethanol and stained with methylene blue. Colonies containing >50 cells were counted. The survival fraction was calculated as: (number of colonies formed ÷ number of cells seeded) for treated samples, normalized to the corresponding value for untreated controls. Synergy was evaluated by Bliss independence using the fraction of affected cells, as described above for the viability assay (see also Supplementary Fig. S5C and Supplementary Fig. S6F and G).

Analysis of clinical samples from cervical and prostate cancers

Gene expression and clinical outcome data of 291 locally advanced cervical cancer patients treated with curative chemoradiotherapy and 94 intermediate- and high-risk prostate cancer patients treated with radical prostatectomy were used. Patient cohorts, treatments, and data acquisition have been described elsewhere [26, 27]. Gene expression data (GEO accession numbers: GSE72723 and GSE146114 for cervix cancer and GSE178631 for prostate cancer) were generated by Illumina Bead Arrays, using total RNA extracted from pretreatment tumor biopsies. Signal measurement and quantile normalization were performed using the software provided by the manufacturer (Illumina Inc.). Log_2-transformed data were used in the analysis. The clinical endpoint for the cervical cancer cohort was progression-free survival, defined as time from diagnosis to disease-related death or first event of relapse. For prostate cancer, biochemical relapse (BCR), assessed by blood level of prostate-specific antigen (PSA), was used as a clinical endpoint. BCR was defined as PSA ≥ 0.2 ng/ml after prostatectomy or as PSA ≥ 2 ng/ml above nadir for four patients receiving postoperative radiation therapy. Clinical markers, including International Society of Urological Pathology (ISUP) grade group and pathological tumor stage (pT) were also assessed for this cohort.

Results

WDR82/PNUTS-PP1 suppresses DNA damage in S-phase after WEE1 inhibition

We previously showed that the WDR82/PNUTS-PP1 complex suppresses T-R conflicts by destabilizing RNAPII, thereby allowing timely removal of RNAPII from chromatin [22]. Furthermore, we have shown that WEE1 inhibition by adavosertib causes DNA damage in S-phase largely through CDK-mediated increased replication initiation [6]. Because elevated origin firing may promote T-R conflicts [8], we thus hypothesized that combining enhanced replication initiation by adavosertib with stabilization of RNAPII on chromatin via depletion of WDR82 would exacerbate DNA damage in replicating cells. Indeed, DNA damage was enhanced in S-phase at 2 and 6 h after adavosertib treatment in WDR82-depleted HeLa cells compared to control siRNA-transfected HeLa cells, as measured by the DNA double strand break marker γH2AX (Fig. 1A and Supplementary Fig. S1A and B). The DNA double-strand break markers phospho-ATM T1989, phospho-DNAPK S2056, and phospho-RPA S4S8 were also enhanced after adavosertib in WDR82-depleted cells (Fig. 1B and C), and this was specific for WDR82 depletion, as it was rescued in cells expressing siRNA-resistant WDR82 (Fig. 1B and C). Furthermore, depletion of PNUTS, the scaffolding component of the WDR82/PNUTS-PP1 complex [18], enhanced DNA damage in S-phase in HeLa and U2OS cells upon adavosertib treatment (Fig. 1D and Supplementary Fig. S1C and D). Depletion of PNUTS also enhanced DNA damage in S-phase after CHK1 inhibition (Supplementary Fig. S1D), which enhances replication initiation by mechanisms distinct from WEE1 inhibition [28, 29]. Whereas WEE1 inhibition strongly increases CDK activity, CHK1 inhibition causes only a minor increase in CDK activity and instead promotes loading of the initiation factor CDC45 through TRESLIN regulation [28, 30]. Moreover, WEE1 inhibition is thought to kill cancer cells by inducing DNA damage during S-phase [31]. Consistent with this, WDR82-depleted cells showed decreased survival compared to control siRNA-transfected cells in the presence of adavosertib (Fig. 1E).

Inhibitors of active transcription suppress replication stress after WEE1 inhibition

Elongating RNAPII is a major obstacle to the replication fork [32]. To further address the role of RNAPII in replication stress after WEE1 inhibition, we added inhibitors of productive RNAPII elongation. In line with our hypothesis that T-R conflicts may contribute to replication stress after WEE1 inhibition, 5,6-dichloro-1-beta-D-ribofuranosylbenzimidazole (DRB) and THZ1 reduced the elevated levels of the DNA double-strand break markers pATM T1989, pDNAPK S2056, and pRPA S4S8. Slight re-

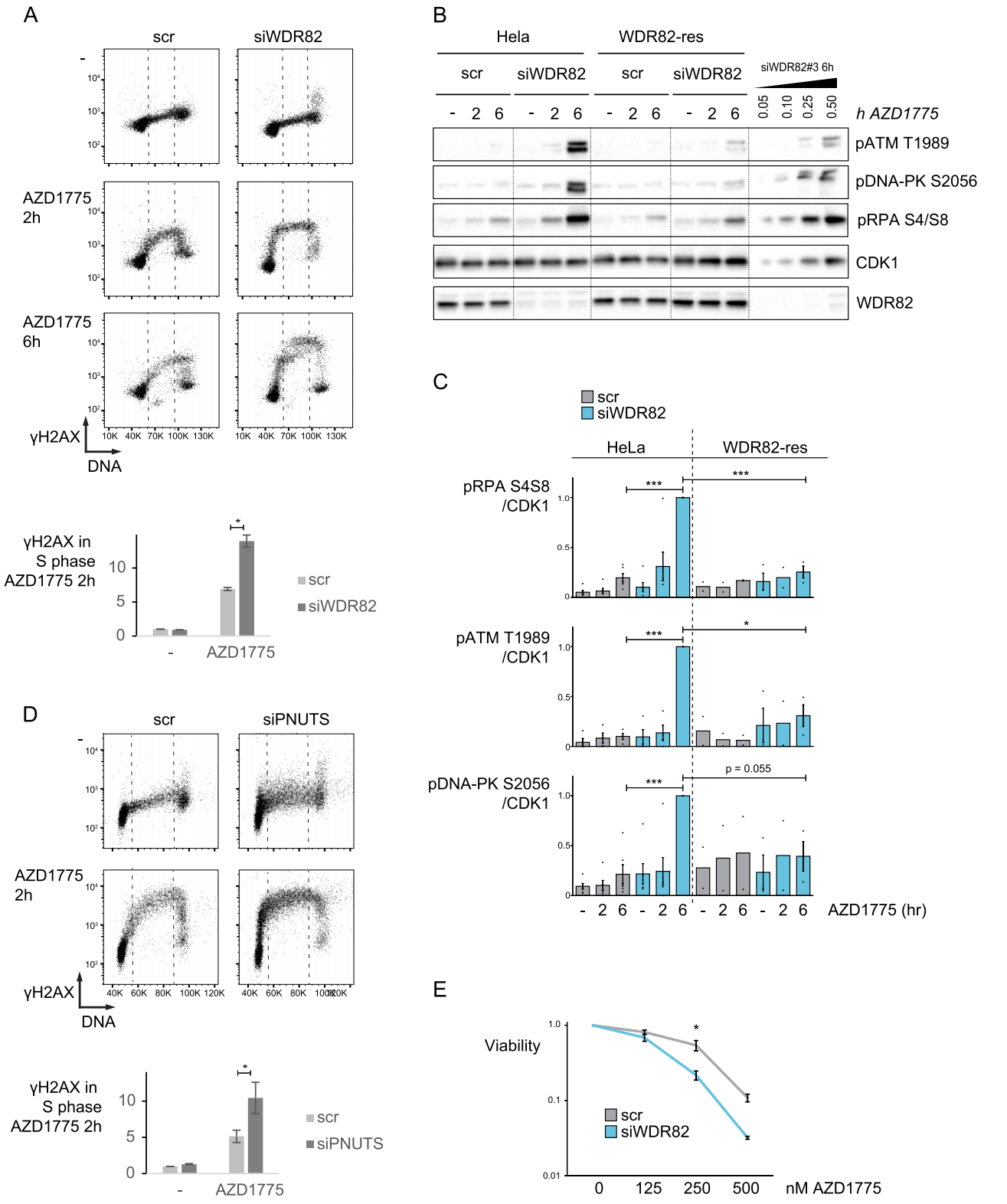

Figure 1. WDR82/PNUTS-PP1 is required to suppress DNA damage in S-phase after WEE1 inhibition. **(A)** Flow cytometry analysis of control siRNA (scr) or WDR82 siRNA (siWDR82) transfected HeLa cells treated with or without 1 μM AZD1775 for 2 or 6 h and stained with the DNA damage marker γH2AX and the DNA stain Hoechst 33258. Dotted lines indicate S-phase. The bar chart shows quantification of median γH2AX levels in S-phase from three independent experiments. **(B)** Western blot analysis of HeLa cells (HeLa) and HeLa cells stably expressing siRNA-resistant WDR82 (WDR82-res). Cells were siRNA-transfected and treated as in A. **(C)** Quantification of pATM T1989, pDNA-PK S2056, and pRPA S4/S8 relative to levels of CDK1 from six (HeLa) or three (WDR82-res) independent experiments, as in B. **(D)** Flow cytometry analysis of scr or PNUTS siRNA (siPNUTS) transfected cells treated with or without 1 μM AZD1775 for 2 h at 48 h after siRNA transfection, and stained with anti-γH2AX and Hoechst 33258. The bar chart shows quantification of median γH2AX levels in S-phase from three independent experiments. **(E)** Relative viability of scr and siWDR82 transfected cells treated with indicated concentrations of adavosertib (AZD1775) for 24 h, assessed by the Cell Titer Glow assay four days later. Inhibitors were added 48 h post-transfection ($n = 3$). Error bars: SEM. $*P < 0.05$, $**P < 0.01$, $***P < 0.001$ (two tailed Student's t-test).

ductions by DRB and THZ1 were also observed for the replication stress markers pCHK1 S345 and pRPA S33, although these decreases did not reach statistical significance (Fig. 2A and B and Supplementary Fig. S2A). Furthermore, DRB and triptolide (TPL) reduced γH2AX levels in S-phase after adavosertib in control and in WDR82-depleted cells (Supplementary Fig. S2B), while having no major effects on cell cycle profiles (Supplementary Fig. S2B and C). Notably, replication stress after WEE1 inhibition is dependent on CDK1/2 activity [6]. As DRB and TPL did not inhibit mitotic entry after adavosertib (Supplementary Fig. S2D), which is also mediated by CDK1/2, DRB and TPL likely do not act by reducing the CDK1/2 activity. On the other hand, in line with the role of CDK7 as a CDK1/2 activating kinase [33], we found that the CDK7 inhibitor THZ1 inhibited CDK1/2 activity as measured by mitotic entry after adavosertib (Supplementary Fig. S2D). Nevertheless, as CDK1/2 activity was not affected by DRB or TPL, the lower DNA damage in S-phase after adavosertib with these inhibitors supports that the elongating RNAPII may contribute to replication stress after WEE1 inhibition.

The transcription elongation factor CDC73 promotes replication stress after WEE1 inhibition

Next, we addressed whether the transcription elongation factor CDC73, a component of the PAF1 transcription elongation complex, was required for the DNA damage after WEE1 inhibition in cells depleted for WDR82. We reasoned that this would likely be the case as we previously found that CDC73 was required for the enhanced stability of RNAPII on chromatin after depletion of PNUTS [22]. Indeed, depletion of CDC73 suppressed DNA damage in S-phase after adavosertib in combination with WDR82 depletion (Fig. 2C and Supplementary Fig. S3A). In line with the reduced DNA damage (also without depleting WDR82), depletion of CDC73 or two other components of the PAF1 complex, PAF1 and CTR9, promoted cell survival after WEE1 inhibition in U2OS cells (Supplementary Fig. S3B). The PAF1 transcription elongation complex thus appears to enhance, while WDR82 suppresses, DNA damage and cell death after WEE1 inhibition. Next, we performed chrRNAseq on cells depleted for WDR82 and/or CDC73 to investigate the opposing roles of these factors after WEE1 inhibition. Consistent with defective transcription termination after WDR82 depletion [19, 20], enhanced readthrough transcription beyond the 3′ end of protein coding genes was observed in WDR82-depleted cells compared to control siRNA-transfected cells (Fig. 2D and E and Supplementary Fig. S3C). Remarkably, co-depletion of CDC73 suppressed this effect (Fig. 2D and E and Supplementary Fig. S3C), paralleling the suppression of S-phase DNA damage observed under the same conditions. Similar results were obtained when analyzing either the top 2000 expressed genes or all expressed genes (Fig. 2D and F (left panel) and Supplementary Fig. S3C and E (left panel)). Interestingly, single depletion of CDC73 produced a modest increase in readthrough (Fig. 2D–F (left panel) and Supplementary Fig. S3C and E (left panel)), suggesting that CDC73 may either promote or inhibit transcription termination depending on context. However, when restricting analysis to genes with pronounced readthrough (log2 ratio > -5), single depletion of CDC73 did not result in increased readthrough (Fig. 2F and Supplementary Fig. S3E; mid panels). Furthermore, the number of genes with very high readthrough (log ratio > -2) increased specifically after WDR82 depletion, but not after CDC73 depletion or WDR82/CDC73 co-depletion (Fig. 2F and S3E; right panels). These findings indicate that WDR82 and CDC73 exert distinct effects on transcription termination, with CDC73 co-depletion suppressing termination defects caused by WDR82 loss. We also examined polyA signal frequency in the chrRNA-seq data for genes with very high readthrough. PolyA signals were reduced in readthrough regions following WDR82 depletion, but not after CDC73 depletion, and were partially rescued by CDC73 co-depletion (Supplementary Fig. S3F). Moreover, analysis of elongating RNAPII (pRNAPII S2) levels on chromatin in single cells by flow cytometry [34] revealed that depletion of WDR82 increased, while depletion or co-depletion of CDC73 decreased, pRNAPII S2 levels in S-phase relative to G1 (Fig. 2G and H and Supplementary Fig. S3G–I). These data further support distinct roles for CDC73 and WDR82 in termination, and suggest that termination is important for the removal of elongating RNAPII from chromatin in S phase. Similar effects on pRNAPII S2 were observed after co-depletion of CDC73 with PNUTS (Fig. 2I and Supplementary Fig. S3G–I). Together, these results suggest that transcription termination reduces the levels of productively elongating RNAPII on chromatin during DNA replication, thereby suppressing T-R conflicts after adavosertib treatment.

Replication stress after WEE1 inhibition is counteracted by transcription termination factors

The above results strongly suggested that impaired transcription termination might explain the enhanced DNA damage in S-phase in cells depleted for WDR82 and PNUTS after WEE1 inhibition. To further investigate this, we measured DNA damage by γH2AX after siRNA-mediated depletion of three additional transcription termination factors. In line with a role for transcription termination in counteracting replication stress after WEE1 inhibition, depletion of the transcription termination factors XRN2, CPSF73, and DDX5 enhanced γH2AX in S-phase after adavosertib, similarly to depletion of WDR82 or PNUTS (Fig. 3A–D and Supplementary Fig. S4A–C). Furthermore, for all five termination factors, co-depletion of CDC73 suppressed the adavosertib-induced DNA damage (Fig. 3C–F and Supplementary Fig. S4C). These results further support that transcription termination counteracts replication stress following WEE1 inhibition.

Combined inhibition of transcription termination with adavosertib synergistically induces DNA damage and reduces cell survival

JTE-607 is a small molecule inhibitor of the CPSF73 transcription termination factor, which promotes readthrough transcription and has anti-cancer effects [35]. We predicted that JTE-607 should act synergistically with WEE1 inhibition to induce DNA damage in S-phase cells. Indeed, combination treatment with JTE-607 and adavosertib enhanced DNA damage in S-phase compared to either monotherapy in HeLa cells (Fig. 4A and B and Supplementary Fig. S4D and E). Furthermore, the combination of siRNA-mediated depletion of WEE1 and JTE-607 treatment led to increased replication-stress markers and S-phase DNA damage

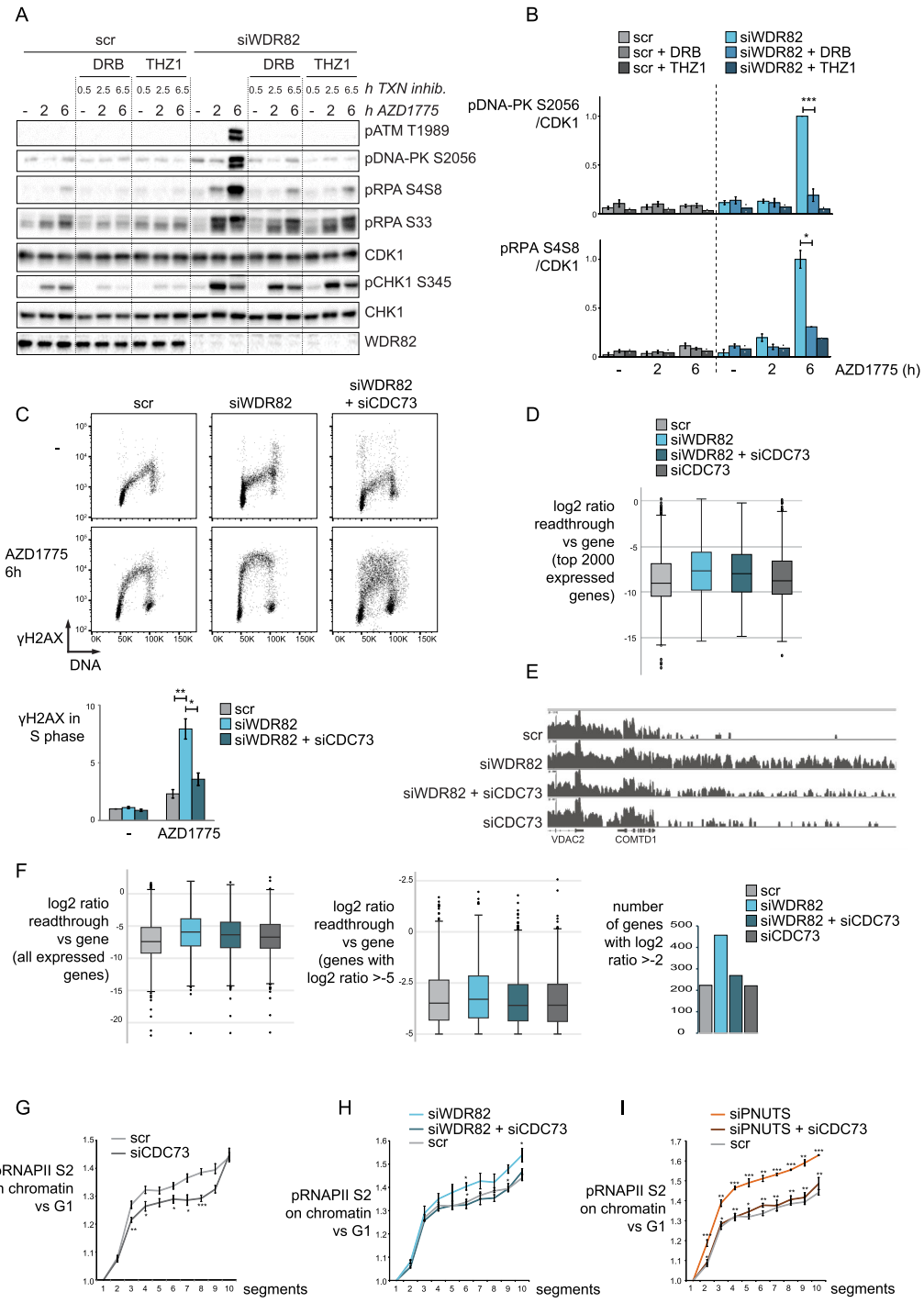

Figure 2. Inhibitors of active transcription or depletion of transcription elongation factor CDC73 suppress DNA damage after WEE1 inhibition. **(A)** Western blot analysis of scr and siWDR82 transfected cells with and without 1 μM adavosertib (AZD1775) for 2 or 6 h. Transcription inhibitors THZ1 and DRB were added 30 min prior to AZD1775. **(B)** Quantifications from experiments as in A, showing pDNA-PK S2056 and pRPA S4S8 versus CDK1. $n = 3$ for DRB-treated and $n = 2$ for THZ1-treated samples. **(C)** Flow cytometry analysis of cells treated with 1 μM AZD1775 at 72h after siRNA transfection and harvested 6 h later. The bar chart shows quantification of S-phase levels of γH2AX from three independent experiments. **(D)** Readthrough analysis from chromatin RNA sequencing experiment of HeLa cells 48 h after siRNA transfection. Box plot showing Log2 ratio of readthrough versus gene from the top 2000 expressed genes. **(E)** Read density profiles from experiments performed as in D showing readthrough from the gene with the biggest difference in readthrough between siWDR82 and scr, visualized in IGV (*VDAC2*: chr10:75 229 310). **(F)** Left: Readthrough analysis from chromatin RNA sequencing as in D for all expressed genes (defined as described in materials and methods). Middle: Readthrough analysis for expressed genes with detectable readthrough (log2 ratio > –5). Right: number of expressed genes with log2 ratio >–2. **(G)** Quantifications of pRNAPII S2 levels on chromatin from flow cytometry analysis, as in Supplementary Fig. S3G. Median levels in segments (shown in Supplementary Fig. S3H) were divided by pRNAPII S2 levels in the internal barcoding control cells. Thereafter, median levels in each segment of the respective siRNA condition (scr or siCDC73) were divided by the median levels in segment 1 (G1). $n = 6$. **(H)** As in G, but for scr, siWDR82, and siWDR82 + siCDC73. $n = 3$. **(I)** As in G, but for scr, siPNUTS, and siPNUTS + siCDC73. $n = 3$. Error bars: SEM. $*P < 0.05$, $**P < 0.01$, $***P < 0.001$ (two tailed Student's t-test). Statistical comparisons in G-I: scr versus siCDC73/siWDR82/siPNUTS; siWDR82 + siCDC73 versus siWDR82; siPNUTS + siCDC73 versus siPNUTS. Results in D-F are from a representative experiment.

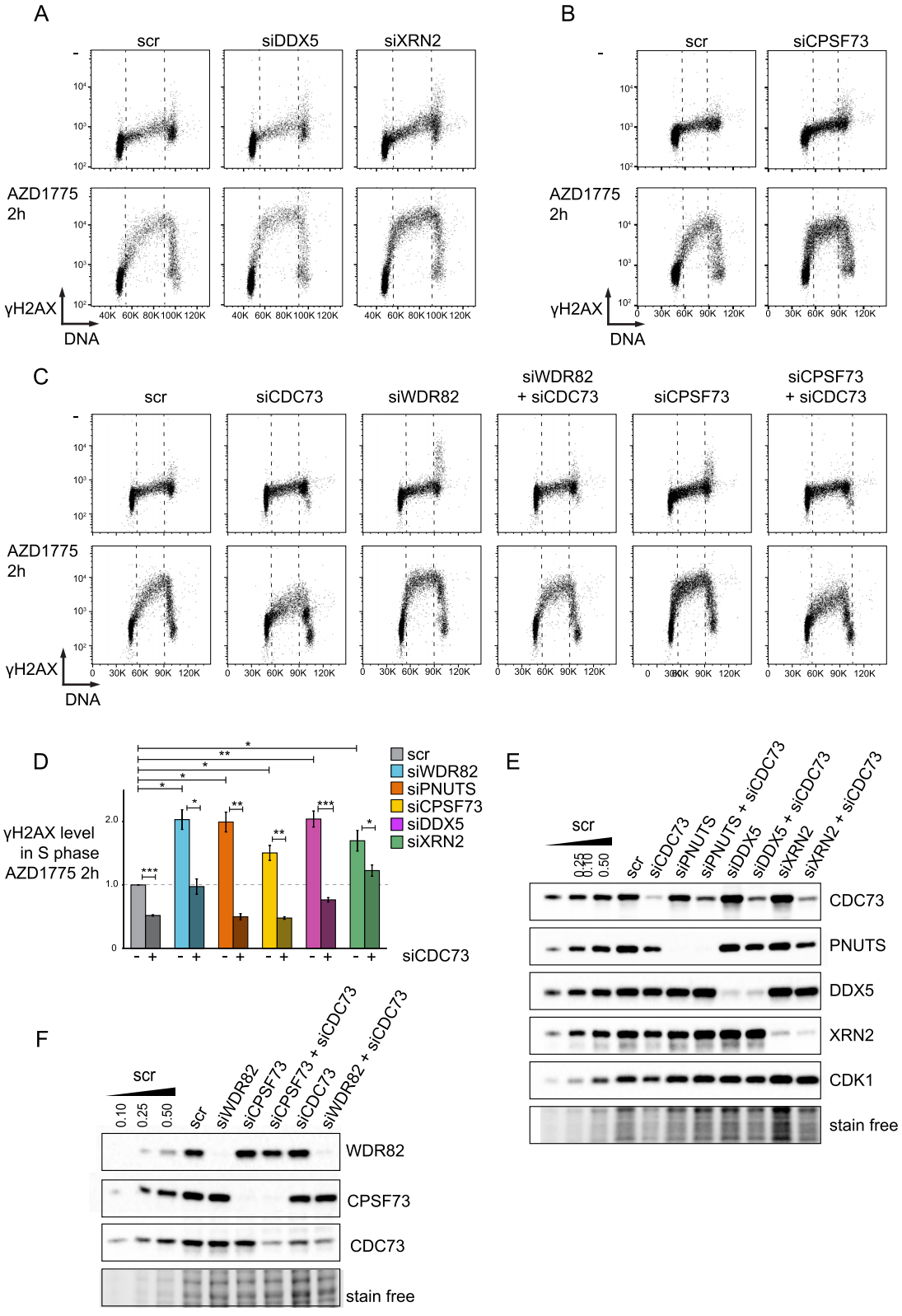

Figure 3. Transcription termination suppresses DNA damage in S-phase after WEE1 inhibition. **(A)** Flow cytometry analysis of cells transfected with scr and siRNA against DDX5 (siDDX5) and XRN2 (siXRN2) with and without 1 μM adavosertib (AZD1775) for 2 h, at 48 h after siRNA transfection. **(B)** As in A, but cells were transfected with siRNA against CPSF73 (siCPSF73). **(C)** As in A, but cells were transfected with scr, siWDR82, and siCPSF73 with and without siRNA against CDC73 (siCDC73). Of note is that cells transfected with siCDC73 in the absence of siWDR82 and siCPSF73 were transfected with only siCDC73 (not in combination with scr). **(D)** Bar chart showing quantifications of median γH2AX levels in S-phase from experiments as in A–C. Error bars represent SEM from ≥3 independent experiments. $*P < 0.05$, $**P < 0.01$, $***P < 0.001$ (two-tailed Student's t-test, except one-sample t-test for comparisons to the normalized sample). **(E)** Western blot showing knockdown levels 48 h after siRNA transfection using the different siRNAs in A–D. **(F)** As in E. Error bars: SEM of ≥3 independent experiments;$*$ $P < 0.05$; $**$ $P < 0.01$; and $***$ $P < 0.001$ (two-tailed Student's t-test).

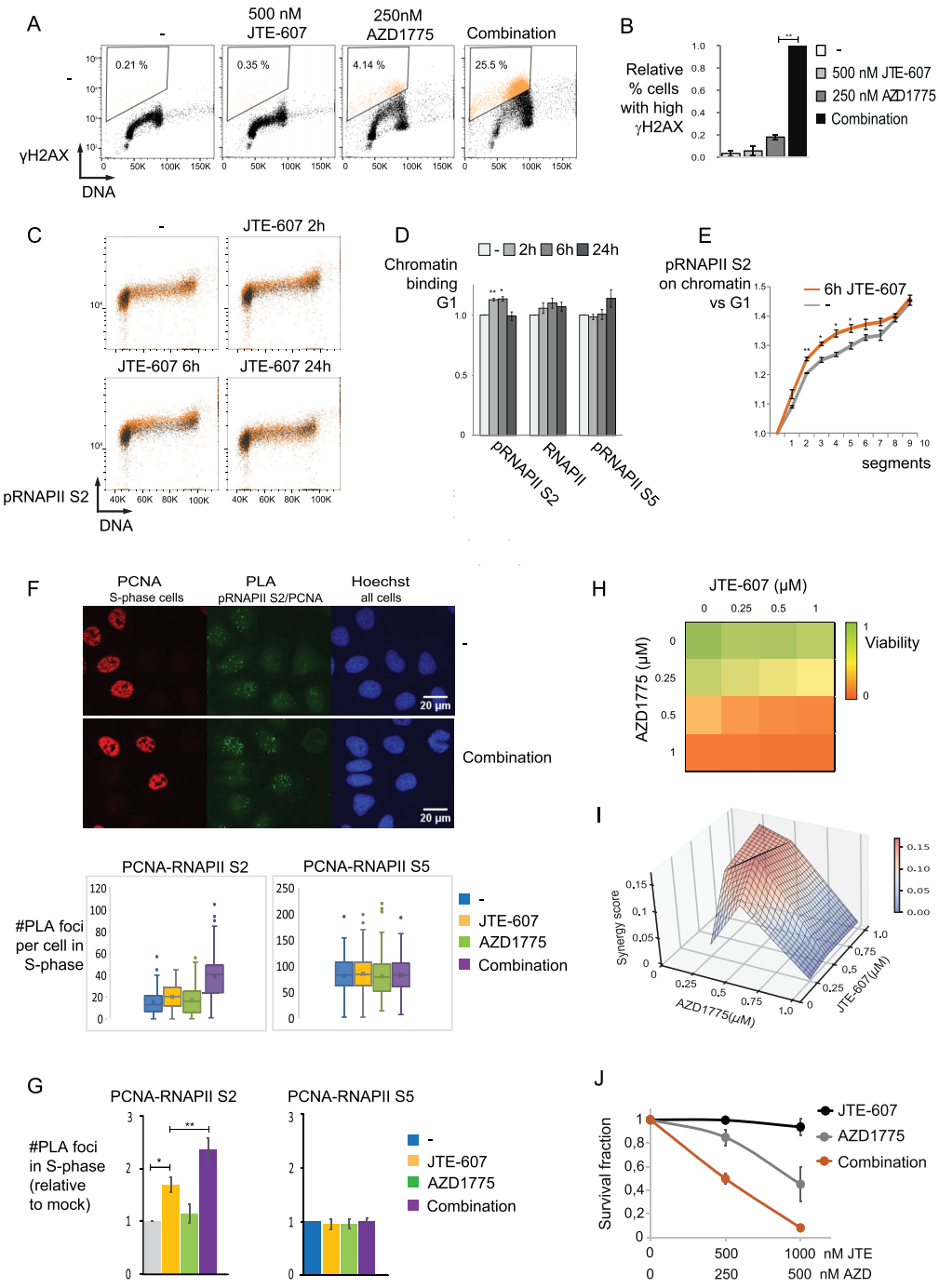

Figure 4. The transcription termination inhibitor JTE-607 synergistically reduces cell survival in combination with adavosertib. **(A)** Flow cytometry analysis of HeLa cells without (-) or with the indicated concentrations of JTE-607 and adavosertib (AZD1775) for 24 h. Numbers indicate γH2AX-positive cells. **(B)** Quantification of the relative proportion of γH2AX-positive cells from three independent experiments as in A. **(C)** Flow cytometry analysis of extracted cells as in Supplementary Fig. S3G of pRNAPII S2 levels on chromatin in HeLa cells without (-) or with 1 μM JTE-607 for 2, 6, and 24 h (orange color). Barcoded mock cells are shown in black color. **(D)** Quantifications from experiments, as in C. Median levels of pRNAPIIS2, RNAPII, and pRNAPII S5 were measured in G1 cells (determined based on DNA content as in Supplementary Fig. S3H), and divided by the median levels in the barcoding control cells in each sample. Levels are shown relative to the untreated (-) G1 cells. $n = 3$. **(E)** Flow cytometry analysis as in Fig. 2G–I of non-treated cells (-) or cells treated with JTE-607 for 6 h (6h JTE-607). $n = 3$.**(F)** Images of pRNAPII S2/PCNA PLA foci in S-phase HeLa cells (PCNA-positive), with nuclei counterstained with Hoechst. Bottom panels show box plots of pRNAPII S2/PCNA and pRNAPII S5/PCNA PLA foci per S-phase cell. Cells were untreated, exposed to 1 μM JTE-607 for 4 h, to 1 μM AZD1775 for 20 min, or to both (1 μM JTE-607 for 4 h with 1 μM AZD1775 added during the last 20 min). Data are from a representative experiment. **(G)** Bar charts show the average of the median PLA foci obtained from three independent experiments, as in F. **(H)** Viability relative to DMSO control from Cell Titer Glow assay of HeLa cells 5 days after treatment with the indicated concentrations of JTE-607 and AZD1775 for 24 h before wash-off and medium replacement. **(I)** Synergy score (excess over BLISS) calculated from viability data from H. **(J)** Clonogenic survival of HeLa cells after 24-h treatment with the indicated concentrations of JTE-607 and adavosertib. Data represent the mean of three independent experiments, each performed in triplicate. (Statistical testing of synergy is shown in Supplementary Fig. S5C.) Error bars represent SEM of ≥three independent experiments;∗ $P < 0.05$; ∗∗ $P < 0.01$; and ∗∗∗ $P < 0.001$.

(Supplementary Fig. S4F,G,H). These findings indicate that the impact of WEE1 inhibition was not a result of off-target effects. Consistent with the role of JTE-607 in inhibiting transcription termination, short-term treatments with JTE-607 enhanced the amount of elongating RNAPII (pRNAPII S2) on chromatin in G1-phase cells (Fig. 4C and D), an effect which was even further enhanced in S-phase at 6h after JTE-607 (Fig. 4E). Inhibition of termination by JTE-607 therefore increases the amount of elongating RNAPII on chromatin, and this effect is especially enhanced in S-phase. Levels of total RNAPII and pRNAPII S5 were also enhanced in S-phase 6h after JTE-607 (Supplementary Fig. S4I–K). However, consistent with the role of JTE-607 in inhibiting transcription termination, at an earlier time of 2 h after JTE-607, the levels of pRNAPII S2 were increased whilst pRNAPII S5 levels, which mark promoter proximal RNAPII [23], were neither enhanced in G1 nor S phase at this time (Fig. 4D and data not shown). We next investigated the spatial proximity between transcription and replication using the proximity ligation assay (PLA) with antibodies against either PCNA and RNAPII S2 or PCNA and RNAPII S5. PLA foci were examined exclusively in S-phase cells, distinguished from other cell cycle phases by the presence of chromatin-bound PCNA (Fig. 4F and Supplementary Fig. S5A and B). Single treatment with JTE-607 moderately increased PCNA-RNAPII S2 proximity, but not PCNA-RNAPII S5 proximity (Fig. 4F and G), suggesting that defective transcription termination after JTE-607 treatment promotes co-localization of transcription and replication. This effect was further enhanced by a short (20 min) treatment with adavosertib (Fig. 4F and G), in line with increased T-R conflicts caused by WEE1 inhibition in combination with JTE-607, and with the involvement of elongating RNAPII (phosphorylated on S2) in these conflicts. Moreover, we investigated the effect of combining JTE-607 with adavosertib on cell survival. The combined treatment synergistically suppressed cell survival, as measured by the Cell titer glow viability assay and clonogenic assays, in the HeLa cervical cancer cells (Fig. 4H–J and Supplementary Fig. S5C).

To address the clinical relevance of JTE-607, we monitored mRNA levels of its target CPSF73 in available patient samples from cervical cancer and prostate cancer. While CPSF73 was expressed in cervical cancer, its levels showed only a weak, non-significant correlation with progression-free survival (Supplementary Fig. S6A). However, in samples from prostate cancer, CPSF73 expression strongly correlated with disease progression, as measured by prostate-specific antigen (PSA) relapse in a cohort of prostate cancer patients undergoing prostatectomy (Fig. 5A). Moreover, high CPSF73 expression also correlated with aggressive disease as measured by ISUP grade and pathological tumor stage (Fig. 5B). We therefore reasoned that combinations of JTE-607 and adavosertib may be a good strategy to target prostate cancer cells. In line with this, combinations of JTE-607 and adavosertib synergistically increased the percentage of cells with high γH2AX in DU-145 and PC3 cells at 24 h after addition of inhibitors (Fig. 5C and D and Supplementary Fig. S6C). Similar to the effects in HeLa cells, elevated DNA damage and replication stress markers (pRPA S4/S8, pRPA S33, and pCHK1 S345) were partially reduced by the addition of DRB (Supplementary Fig. S6D). Moreover, JTE-607 in combination with adavosertib synergistically lowered cell survival compared to either treatment alone (Fig. 5E–G and Supplementary Fig. S6E–G).

Discussion

T-R conflicts may contribute to tumor progression [36, 37] and provide a cancer-specific vulnerability. Nevertheless, the mechanisms underlying T-R conflicts are not fully understood, and there are currently few therapeutic strategies that target such conflicts. In this work, we find that inhibiting WEE1 kinase combined with inhibition of transcription termination synergistically increases DNA damage and reduces cancer cell viability. We propose a model where enhanced replication initiation by WEE1 inhibition combined with defective transcription termination leads to DNA damage and cancer cell death due to T-R conflicts (Fig. 5J).

This model is supported by multiple lines of evidence. Firstly, siRNA-mediated depletion of five different termination factors, which stimulate transcription termination by varying mechanisms, or JTE-607, an inhibitor of transcription termination, promoted DNA damage in S-phase after WEE1 inhibition by adavosertib. This was accompanied by reduced cell survival, as seen for adavosertib in combination with depletion of WDR82 or the termination inhibitor JTE-607. Furthermore, adavosertib-induced S-phase DNA damage after depletion of the termination factors was suppressed by co-depletion of the transcription elongation factor CDC73, which also partially rescued the defective transcription termination after WDR82 depletion. Depletion of CDC73 also promoted cell survival after adavosertib. Moreover, co-treatment with JTE-607 and adavosertib selectively increased PCNA-RNAPII S2 proximity, but not PCNA-RNAPII S5 proximity, supporting the involvement of T-R conflicts and indicating that elongating, rather than promoter proximal, RNAPII mediates these effects. Together, these results thus underline the importance of transcription termination in suppression of T-R conflicts [1, 10, 38, 39, 40], and highlight that transcription termination becomes even more important upon deregulated replication initiation. Interestingly, a recent study revealed that dormant origins frequently fire at or just downstream of transcription termination sites and are a source for T-R conflicts in BRCA2 depleted cells [41]. As WEE1 inhibition promotes dormant origin firing, Wee1 inhibition may thus enhance collisions at termination sites. Such collisions likely escalate upon deregulated transcription termination. On the other hand, additional mechanisms may also contribute. For example, JTE-607 also suppresses cleavage and polyadenylation, which, by depletion of WDR33, was shown to give defects in gene-gating, thereby causing replication stress at the nuclear periphery [42].

Our results suggest elongating RNAPII is of particular importance in T-R conflicts. Indeed, depletion of CDC73 suppressed pRNAPII S2 on chromatin specifically in S-phase and also reduced the adavosertib-induced DNA damage in S-phase. Conversely, depletion of termination factors enhanced pRNAPII S2 on chromatin in S-phase and enhanced DNA damage in S-phase after adavosertib. We further find that transcription termination is likely a mechanism removing elongating RNAPII during normal DNA replication, as depletion of several of the termination factors, or short-term treatment with JTE-607, enhanced pRNAPII S2 on chromatin specifically in S-phase. In addition, short-term treatment with JTE-607 increased the proximity between pRNAPII S2 and PCNA. However, DNA damage was not strongly induced by inhibition of termination alone, but depended on co-treatment with adavosertib, indicating that T-R conflicts arising from JTE-

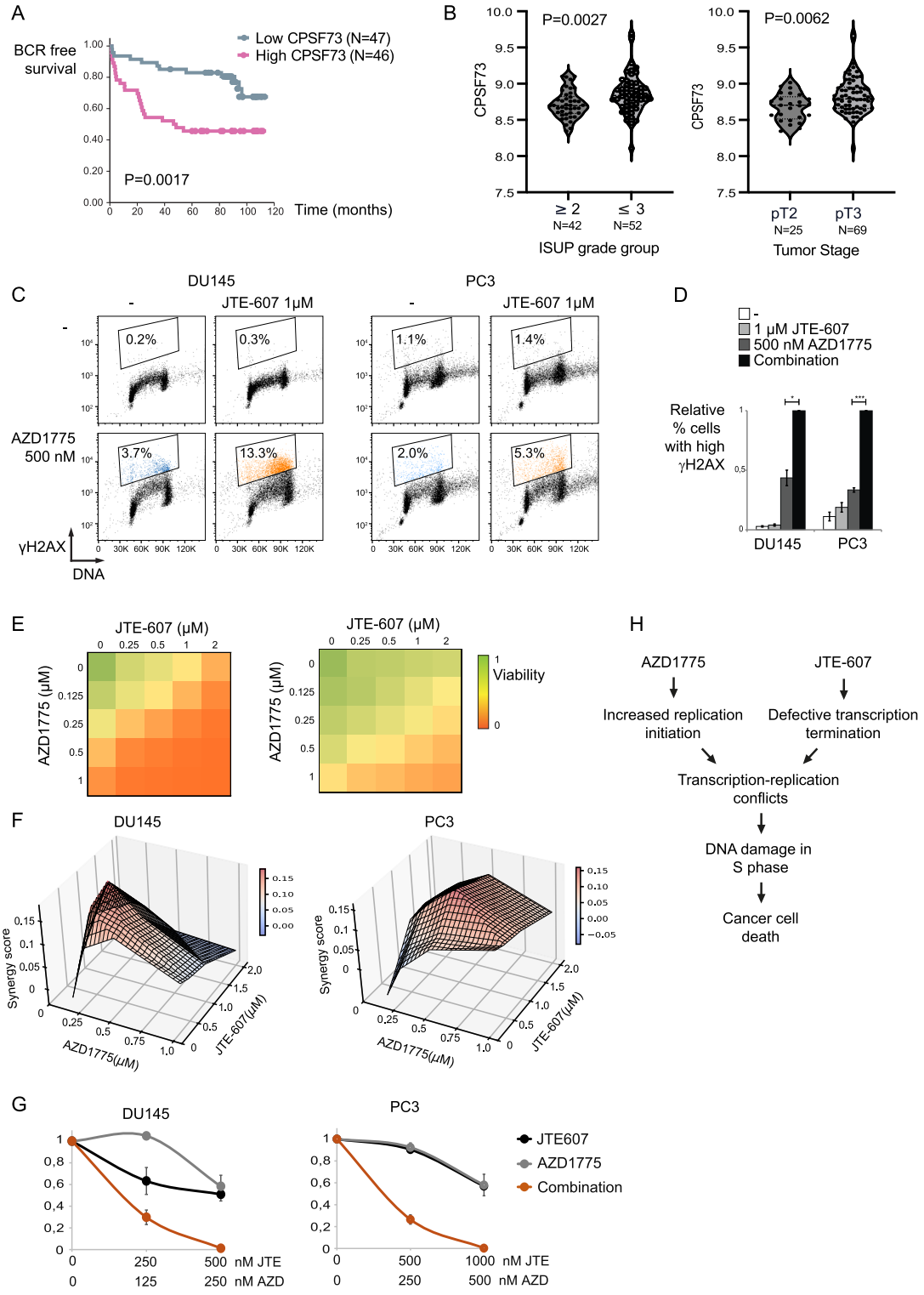

Figure 5. Combined targeting of transcription termination with WEE1 synergistically reduces cell survival in prostate cancer cells. **(A)** Kaplan-Meier plot showing BCR-free survival of prostate cancer patients vs time after prostatectomy. Patients were grouped into two by the median CPSF73 expression based on Illumina Bead Array gene expression data. $n = 93$. **(B)** CPSF73 levels versus ISUP grade group (left) and pathological tumor stage (right) in prostate cancer patients. $n = 94$. **(C)** Flow cytometry analysis of DU145 cells (left) and PC3 cells (right) without (-) or with JTE-607 (1 μM) and adavosertib (AZD1775) (500 nM) for 24 h. Regions indicate percentage cells with high γH2AX levels. **(D)** Quantifications from experiments, as in C, showing average % cells with high γH2AX as determined by the regions shown in C. Results are shown relative to the percentage of cells with high γH2AX after treatment with JTE-607 and AZD1775. $n = 3$. **(E)** Average viability relative to DMSO control from Cell Titer Glow assays of DU145 cells (left) and PC3 cells (right) treated with the indicated concentrations of JTE-607 and AZD1775 for 5 days. $n = 3$. **(F)** Average synergy score (excess over BLISS) calculated from viability data from E. **(G)** Clonogenic survival of DU145 cells (left) and PC3 cells (right) after treatment with the indicated concentrations of JTE-607 and adavosertib. Data represent the mean of three independent experiments, each performed in triplicate. **(H)** Working model. See main text for details. Error bars represent SEM of ≥three independent experiments. $* P < 0.05$; $** P < 0.01$; and $*** P < 0.001$. Statistical testing of synergy in F and G is shown in Supplementary Fig. S6E and Supplementary Fig. S6G.

607 alone are mostly resolved. This suggests that regulation of both transcription and replication contributes to suppression of T-R conflicts, and defective transcription termination alone is not sufficient to cause massive DNA damage.

A central role for elongating RNAPII in T-R conflicts is in line with a study from *Saccharomyces cerevisiae* [32], where deletion of the transcription elongation factors Spt2, Spt5, or Leo1 of the PAF1 complex suppressed replication fork arrest in cells deficient for Sen1, the homologue of Senataxin, which is involved in transcription termination. Notably, inhibition of the PAF1 complex has conversely been shown to promote R-loop accumulation occurring at promoter proximal regions [43]. This argues that the PAF1 complex may either promote or suppress T-R conflicts. As the PAF1 complex enhances release from promoter proximal pausing [43, 44], if the T-R conflicts are caused by promoter proximal RNAPII, the PAF1 complex may play a suppressive role. On the other hand, if, as in our study, the T-R conflicts are caused by defective termination, the PAF1 complex promotes T-R conflicts. As termination and elongation kinetically compete [21], and loss of the PAF1 complex reduces the elongation rate [45], depletion of PAF1 likely rescues defects in termination by slowing down elongation. Supporting the latter, co-depletion of CDC73 partially rescued read-through transcription after depletion of WDR82.

Combined treatment of JTE-607 with adavosertib may be especially relevant for the treatment of patients with metastatic prostate cancer, where curative treatments currently do not exist, and new treatment strategies are urgently needed. Supporting that such combinations are a viable strategy in metastatic prostate cancer, we found that levels of the JTE-607 target CPSF73 strongly correlated with aggressiveness in prostate cancer. Higher CPSF73 levels may thus be beneficial for tumor progression. In light of our own results, an explanation for this might be that enhanced transcription termination could suppress T-R conflicts and thus allow cancer cells to deal with a higher proliferative rate. On the other hand, defective transcription termination correlated with aggressiveness in clear cell renal cell carcinoma, where longer readthrough products caused aberrant expression of cancer genes [46]. Moreover, sensitivity to JTE-607 has been shown to correlate better with the rate of proliferation than cleavage and polyadenylation activity [47], suggesting the main determining factor for whether cells are sensitive to JTE-607 is whether they are replicating. In line with our own results, in the latter study, JTE-607 was shown to synergize with replication stress-inducing agents such as inhibitors of ATR and topoisomerases I and II [47], though notably WEE1 inhibitors were not addressed.

Our study provides further insight into determinants of sensitivity to WEE1 inhibition that may inform future biomarker development and combination strategies. Loss of CDC73, which is common in parathyroid carcinoma [48], likely confers resistance to WEE1 inhibition. Likewise, loss-of-function mutations of CTR9, common in Wilms tumor [49], are expected to promote resistance. In contrast, cancer-associated mutations in the termination factor XRN2 [50] may sensitize tumors to WEE1 inhibition. Consistent with a broader role for termination defects in cancer, increased transcriptional readthrough was found in colon cancers relative to matched non-neoplastic tissues [51]. Readthrough was further elevated after exposure to the topoisomerase inhibitor camptotechin [51], which synergizes with WEE1 inhibition [52]. In light of our findings, camptothecin-induced termination defects may therefore contribute to this synergy.

Our work describes a new way to target T-R conflicts for cancer treatment by combining two drugs that suppress transcription termination and enhance replication initiation, respectively. In so doing, it opens up for further studies where inhibitors of transcription-related pathways to suppress T-R conflicts can be combined with agents that enhance replication initiation, such as WEE1 inhibitors. Furthermore, our results support that transcription termination can be a target for cancer treatment. To date, only one inhibitor of transcription termination exists; this remains a relatively unexplored area of cancer research with high potential.

Acknowledgements

We thank the Flow Cytometry Core Facility, the Advanced Light Microscopy Core Facility, and the Genomics Core Facility at the Institute for Cancer Research, Oslo University Hospital, for helpful assistance, Chloe Müller for technical assistance, Drs. Ragnhild A. Lothe and Kaja C.G. Berg for an earlier analysis, Drs. Alfonso Urbanucci and Nikolai Engedal for providing cell lines, and Dr. Claus Storgaard Sørensen for critical reading of the manuscript.

Author contributions: H.B.L. (Conceptualization [lead], Formal Analysis [equal], Funding acquisition [supporting], Investigation [lead], Methodology [lead], Supervision [equal], Visualization [equal], Writing – original draft [lead], Writing – review & editing [supporting], L.E.S. (Investigation [equal], Methodology [supporting], Writing – review & editing [supporting], L.T.E.B. (Investigation [supporting], Methodology [supporting], Writing – review & editing [supporting], S.H. (Investigation [supporting], Methodology [supporting], Writing – review & editing [supporting], L.V.B. (Investigation [supporting], Writing – review & editing [supporting], L.L. (Investigation [supporting], Methodology [supporting], Writing – review & editing [supporting], C.L.-A. (Formal Analysis [supporting], Methodology [supporting], Writing – review & editing [supporting], C.K. (Formal Analysis [supporting], Methodology [supporting], Writing – review & editing [supporting], H.L. (Data curation [supporting], Supervision [supporting], Writing – review & editing [supporting], C.S.F. (Formal Analysis [supporting], Writing – review & editing [supporting], T.H. (Data curation [supporting], Formal Analysis [supporting], Writing – review & editing [supporting], T.C.H. (Conceptualization [supporting], Supervision [supporting], Writing – review & editing [supporting], R.G.S. (Conceptualization [lead], Formal Analysis [lead], Funding acquisition [lead], Investigation [supporting], Methodology [supporting], Project administration [lead], Resources [lead], Supervision [lead], Visualization [equal], Writing – original draft [lead], Writing – review & editing [lead].

Supplementary data

Supplementary data is available at NAR online.

Conflict of interest

None declared.

Funding

We are grateful for funds from the Norwegian Research Council (275918), Simon Fougner Hartmann Family Foundation, Fridtjof Nansens Fond til Videnskabens Fremme, Familien Blix Fond, Anders Jahres Fond, and the Norwegian Cancer Society (245570). Funding to pay the Open Access publication charges for this article was provided by Internal funds, Oslo University Hospital.

Data availability

The data underlying this article will be shared on reasonable request to the corresponding author. GEO accession numbers for the cervix cancer: GSE72723 and GSE146114.GEO accession numbers for the prostate cancer: GSE178631.GEO accession number for the chrRNAseq data: GSE312256.

References

1. Gomez-Gonzalez B, Aguilera A. Transcription-mediated replication hindrance: a major driver of genome instability. *Genes Dev* 2019;33:1008–26. https://doi.org/10.1101/gad.324517.119
2. Bowry A, Kelly RDW, Petermann E. Hypertranscription and replication stress in cancer. *Trends Cancer* 2021;7:863–77. https://doi.org/10.1016/j.trecan.2021.04.006
3. Liu ZS, Sinha S, Bannister M *et al.* R-Loop Accumulation in Spliceosome Mutant Leukemias Confers Sensitivity to PARP1 Inhibition by Triggering Transcription-Replication Conflicts. *Cancer Res* 2024;84:577–97. https://doi.org/10.1158/0008-5472.CAN-23-3239
4. Gu L, Li M, Li CM *et al.* Small molecule targeting of transcription-replication conflict for selective chemotherapy. *Cell Chem Biol* 2023;30:1235–47. https://doi.org/10.1016/j.chembiol.2023.07.001
5. da Costa A, Chowdhury D, Shapiro GI *et al.* Targeting replication stress in cancer therapy. *Nat Rev Drug Discov* 2023;22:38–58. https://doi.org/10.1038/s41573-022-00558-5
6. Beck H, Nähse-Kumpf V, Larsen MS *et al.* Cyclin-dependent kinase suppression by WEE1 kinase protects the genome through control of replication initiation and nucleotide consumption. *Mol Cell Biol* 2012;32:4226–36. https://doi.org/10.1128/MCB.00412-12
7. Moiseeva TN, Qian C, Sugitani N *et al.* 2019; WEE1 kinase inhibitor AZD1775 induces CDK1 kinase-dependent origin firing in unperturbed G1- and S-phase cells. *Proc Natl Acad Sci USA* 116:23891–3.
8. Jones RM, Mortusewicz O, Afzal I *et al.* Increased replication initiation and conflicts with transcription underlie Cyclin E-induced replication stress. *Oncogene* 2013;32:3744–53. https://doi.org/10.1038/onc.2012.387
9. Hamilton EP, Falchook GS, Wang JS *et al.* Adavosertib in Combination with Olaparib in Patients with Refractory Solid Tumors: an Open-Label, Dose-Finding, and Dose-Expansion Phase Ib Trial. *Targ Oncol* 2024;19:879–92. https://doi.org/10.1007/s11523-024-01102-8
10. Washburn RS, Gottesman ME. Transcription termination maintains chromosome integrity. *Proc Natl Acad Sci USA* 2011; 108:792–7.
11. Rodríguez-Molina JB, West S, Passmore LA. Knowing when to stop: transcription termination on protein-coding genes by eukaryotic RNAPII. *Mol Cell* 2023;83:404–15. https://doi.org/10.1016/j.molcel.2022.12.021
12. Nojima T, Proudfoot NJ. Mechanisms of lncRNA biogenesis as revealed by nascent transcriptomics. *Nat Rev Mol Cell Biol* 2022;23:389–406. https://doi.org/10.1038/s41580-021-00447-6
13. Kamieniarz-Gdula K, Proudfoot NJ. Transcriptional control by premature termination: a forgotten mechanism. *Trends Genet* 2019;35:553–64. https://doi.org/10.1016/j.tig.2019.05.005
14. Liu H, Moore CL. On the cutting edge: regulation and therapeutic potential of the mRNA 3′ end nuclease. *Trends Biochem Sci* 2021;46:772–84. https://doi.org/10.1016/j.tibs.2021.04.003
15. Skourti-Stathaki K, Proudfoot NJ, Gromak N. Human senataxin resolves RNA/DNA hybrids formed at transcriptional pause sites to promote Xrn2-dependent termination. *Mol Cell* 2011;42:794–805. https://doi.org/10.1016/j.molcel.2011.04.026
16. Mersaoui SY, Yu Z, Coulombe Y *et al.* Arginine methylation of the DDX5 helicase RGG/RG motif by PRMT5 regulates resolution of RNA:DNA hybrids. *EMBO J* 2019;38:e100986. https://doi.org/10.15252/embj.2018100986
17. Cortazar MA, Sheridan RM, Erickson B *et al.* Control of RNA Pol II Speed by PNUTS-PP1 and Spt5 dephosphorylation facilitates termination by a "Sitting Duck Torpedo" Mechanism. *Mol Cell*;2019;76:896–908. https://doi.org/10.1016/j.molcel.2019.09.031
18. Lee JH, You J, Dobrota E *et al.* Identification and characterization of a novel human PP1 phosphatase complex. *J Biol Chem* 2010;285:24466–76. https://doi.org/10.1074/jbc.M110.109801
19. Estell C, Davidson L, Eaton JD *et al.* A restrictor complex of ZC3H4, WDR82, and ARS2 integrates with PNUTS to control unproductive transcription. *Mol Cell* 2023;83:2222–2239.e5. https://doi.org/10.1016/j.molcel.2023.05.029
20. Austenaa LM, Barozzi I, Simonatto M *et al.* Transcription of mammalian cis-regulatory elements is restrained by actively enforced early termination. *Mol Cell* 2015;60:460–74. https://doi.org/10.1016/j.molcel.2015.09.018
21. Fong N, Brannan K, Erickson B *et al.* Effects of transcription elongation rate and Xrn2 exonuclease activity on RNA polymerase II termination suggest widespread kinetic competition. *Mol Cell* 2015;60:256–67. https://doi.org/10.1016/j.molcel.2015.09.026
22. Landsverk HB, Sandquist LE, Bay LTE *et al.* WDR82/PNUTS-PP1 prevents transcription-replication conflicts by promoting RNA polymerase II degradation on chromatin. *Cell Rep* 2020;33:108469. https://doi.org/10.1016/j.celrep.2020.108469
23. Bay LTE, Stokke T, Syljuåsen RG *et al.* Analysis of RNA polymerase II chromatin binding by flow cytometry. *Bio-protocol* 2023;13:e4659. https://doi.org/10.21769/BioProtoc.4659
24. Dobin A, Davis CA, Schlesinger F *et al.* STAR: ultrafast universal RNA-seq aligner. *Bioinformatics* 2013;29:15–21. https://doi.org/10.1093/bioinformatics/bts635
25. Roth SJ, Heinz S, Benner C. ARTDeco: automatic readthrough transcription detection. *BMC Bioinf* 2020;21:214. https://doi.org/10.1186/s12859-020-03551-0
26. Salberg UB, Skingen VE, Fjeldbo CS *et al.* A prognostic hypoxia gene signature with low heterogeneity within the dominant tumour lesion in prostate cancer patients. *Br J Cancer* 2022;127:321–8. https://doi.org/10.1038/s41416-022-01782-x
27. Fjeldbo CS, Julin CH, Lando M *et al.* Integrative analysis of DCE-MRI and gene expression profiles in construction of a gene classifier for assessment of hypoxia-related risk of chemoradiotherapy failure in cervical cancer. *Clin Cancer Res* 2016;22:4067–76. https://doi.org/10.1158/1078-0432.CCR-15-2322
28. Hauge S, Naucke C, Hasvold G *et al.* Combined inhibition of Wee1 and Chk1 gives synergistic DNA damage in S-phase due to distinct regulation of CDK activity and CDC45 loading. *Oncotarget* 2017;8:10966–79. https://doi.org/10.18632/oncotarget.14089
29. Syljuåsen RG, Sørensen CS, Hansen LT *et al.* Inhibition of human Chk1 causes increased initiation of DNA replication, phosphorylation of ATR targets, and DNA breakage. *Mol Cell Biol* 2005;25:3553–62. https://doi.org/10.1128/MCB.25.9.3553-3562.2005
30. Guo C, Kumagai A, Schlacher K *et al.* Interaction of Chk1 with Treslin negatively regulates the initiation of chromosomal DNA

replication. *Mol Cell* 2015;57:492–505. https://doi.org/10.1016/j.molcel.2014.12.003
31. Guertin AD, Li J, Liu Y *et al.* Preclinical evaluation of the WEE1 inhibitor MK-1775 as single-agent anticancer therapy. *Mol Cancer Ther* 2013;12:1442–52. https://doi.org/10.1158/1535-7163.MCT-13-0025
32. Zardoni L, Nardini E, Brambati A *et al.* Elongating RNA polymerase II and RNA:DNA hybrids hinder fork progression and gene expression at sites of head-on replication-transcription collisions. *Nucleic Acids Res* 2021;49:12769–84. https://doi.org/10.1093/nar/gkab1146
33. Larochelle S, Merrick KA, Terret ME *et al.* Requirements for Cdk7 in the assembly of Cdk1/cyclin B and activation of Cdk2 revealed by chemical genetics in human cells. *Mol Cell* 2007;25:839–50. https://doi.org/10.1016/j.molcel.2007.02.003
34. Bay LTE, Syljuåsen RG, Landsverk HB. A novel, rapid and sensitive flow cytometry method reveals degradation of promoter proximal paused RNAPII in the presence and absence of UV. *Nucleic Acids Res* 2022;50:e89. https://doi.org/10.1093/nar/gkac434
35. Ross NT, Lohmann F, Carbonneau S *et al.* CPSF3-dependent pre-mRNA processing as a druggable node in AML and Ewing's sarcoma. *Nat Chem Biol* 2020;16:50–9. https://doi.org/10.1038/s41589-019-0424-1
36. Bayona-Feliu A, Herrera-Moyano E, Badra-Fajardo N *et al.* The chromatin network helps prevent cancer-associated mutagenesis at transcription-replication conflicts. *Nat Commun* 2023;14:6890. https://doi.org/10.1038/s41467-023-42653-0
37. Stork CT, Bocek M, Crossley MP *et al.* Co-transcriptional R-loops are the main cause of estrogen-induced DNA damage. *eLife* 2016;5:e17548. https://doi.org/10.7554/eLife.17548
38. Promonet A, Padioleau I, Liu Y *et al.* Topoisomerase 1 prevents replication stress at R-loop-enriched transcription termination sites. *Nat Commun* 2020;11:3940. https://doi.org/10.1038/s41467-020-17858-2
39. Gaillard H, Aguilera A. Cleavage factor I links transcription termination to DNA damage response and genome integrity maintenance in Saccharomyces cerevisiae. *PLoS Genet* 2014;10:e1004203. https://doi.org/10.1371/journal.pgen.1004203
40. Morales JC, Richard P, Patidar PL *et al.* XRN2 links transcription termination to DNA damage and replication stress. *PLoS Genet* 2016;12:e1006107. https://doi.org/10.1371/journal.pgen.1006107
41. Goehring L, Keegan S, Lahiri S *et al.* Dormant origin firing promotes head-on transcription-replication conflicts at transcription termination sites in response to BRCA2 deficiency. *Nat Commun* 2024;15:4716. https://doi.org/10.1038/s41467-024-48286-1
42. Teloni F, Michelena J, Lezaja A *et al.* Efficient pre-mRNA cleavage prevents replication-stress-associated genome instability. *Mol Cell* 2019;73:670–83. https://doi.org/10.1016/j.molcel.2018.11.036
43. Shivji MKK, Renaudin X, Ç W *et al.* BRCA2 regulates transcription elongation by RNA polymerase II to prevent R-Loop accumulation. *Cell Rep* 2018;22:1031–9. https://doi.org/10.1016/j.celrep.2017.12.086
44. Chen FX, Woodfin AR, Gardini A *et al.* PAF1, a molecular regulator of promoter-proximal pausing by RNA polymerase II. *Cell* 2015;162:1003–15. https://doi.org/10.1016/j.cell.2015.07.042
45. Hou L, Wang Y, Liu Y *et al.* Paf1C regulates RNA polymerase II progression by modulating elongation rate. *Proc Natl Acad Sci USA* 2019; 116:14583–92.
46. Grosso AR, Leite AP, Carvalho S *et al.* Pervasive transcription read-through promotes aberrant expression of oncogenes and RNA chimeras in renal carcinoma. *eLife* 2015;4:e09214. https://doi.org/10.7554/eLife.09214
47. Cui Y, Wang L, Ding Q *et al.* Elevated pre-mRNA 3′ end processing activity in cancer cells renders vulnerability to inhibition of cleavage and polyadenylation. *Nat Commun* 2023;14:4480. https://doi.org/10.1038/s41467-023-39793-8
48. Pandya C, Uzilov AV, Bellizzi J *et al.* Genomic profiling reveals mutational landscape in parathyroid carcinomas. *JCI Insight* 2017;2:e92061. https://doi.org/10.1172/jci.insight.92061
49. Hanks S, Perdeaux ER, Seal S *et al.* Germline mutations in the PAF1 complex gene CTR9 predispose to Wilms tumour. *Nat Commun* 2014;5:4398. https://doi.org/10.1038/ncomms5398
50. Patidar PL, Viera T, Morales JC *et al.* XRN2 interactome reveals its synthetic lethal relationship with PARP1 inhibition. *Sci Rep* 2020;10:14253. https://doi.org/10.1038/s41598-020-71203-7
51. Abe K, Maunze B, Lopez PA *et al.* Downstream-of-gene (DoG) transcripts contribute to an imbalance in the cancer cell transcriptome. *Sci Adv* 2024;10:eadh9613. https://doi.org/10.1126/sciadv.adh9613
52. Hirai H, Arai T, Okada M *et al.* MK-1775, a small molecule Wee1 inhibitor, enhances anti-tumor efficacy of various DNA-damaging agents, including 5-fluorouracil. *Cancer Biol Ther* 2010;9:514–22. https://doi.org/10.4161/cbt.9.7.11115

Received: September 6, 2024. **Revised:** December 4, 2025. **Accepted:** December 11, 2025